Journal of Alloys and Compounds 509 (2011) 6677–6682

Contents lists available at ScienceDirect

Journal of Alloys and Compounds

journal homepage: www.elsevier.com/locate/jallcom

Chemical synthesis and electrochemical analysis of nickel cobaltite nanostructures for supercapacitor applications

Rahul R. Salunkhe[a], Kihun Jang[a], Hyunuk Yu[a], Seongil Yu[a], Thothadri Ganesh[b], Sung-Hwan Han[b,c], Heejoon Ahn[a,c,*]

[a] Department of Organic and Nano Engineering and Institute of Nano Science and Technology, Hanyang University, Seoul 133-791, Republic of Korea
[b] Department of Chemistry, Hanyang University, Seoul 133-791, Republic of Korea
[c] Asian Research Network Program, Hanyang University, Seoul 133-791, Republic of Korea

ARTICLE INFO

Article history:
Received 20 December 2010
Received in revised form 19 March 2011
Accepted 23 March 2011
Available online 31 March 2011

Keywords:
Oxide materials
Thin films
Chemical synthesis
Supercapacitor

ABSTRACT

Nickel cobaltite ($NiCo_2O_4$) films containing nanorods and nanoflakes are synthesized on indium tin oxide (ITO) substrates by a chemical bath deposition method and calcination process at 300 °C for 3 h. The $NiCo_2O_4$/ITO films are used as electrodes for supercapacitor applications, and electrochemical properties of the $NiCo_2O_4$ nanostructures are examined by cyclic voltammetry and charge–discharge experiments. $NiCo_2O_4$ nanorods exhibit the largest specific capacitance, with a value of 490 F g^{-1} at energy and power densities of 45 Wh kg^{-1} and 2 kW kg^{-1}, respectively. This is significantly better than the performance of $NiCo_2O_4$ nanoflakes. Cycle-life tests show that the specific capacitance of $NiCo_2O_4$ is stable even after 1000 cycles, indicating its high potential for supercapacitor applications. The low cost and environmental friendliness of $NiCo_2O_4$ nanorods, coupled with its high supercapacitor performance, offer advantages over other transition metal oxides used for supercapacitors.

1. Introduction

In the case of high energy and high power density electrochemical capacitors, so called supercapacitors, three-dimensional and mesoporous structures are desirable for electrode materials because the porous structures offer large surface areas for electrode–electrolyte reactions and enable electrolytes easily to penetrate through the entire electrode matrix [1–7]. Hence, there has been a large amount of research interest in the preparation of metal or metal oxide nanostructures with controlled interior nanospaces for supercapacitor applications. Supercapacitors can be classified into two types based on the charge-storage mechanism: electrical double-layer capacitors (EDLCs) and pseudocapacitors [8]. The pseudocapacitance can be generated from electroactive materials possessing multiple oxidation states. Transition metal oxides belong to this class of materials and have attracted a great deal of attention for this application. Among various transition metal oxides, ruthenium oxide is one of the most promising pseudocapacitor electrode materials because of its superior electrochemical response [9]. However, despite the superior performance of ruthenium oxide, it is still limited in industrial supercapacitor applications due to its high cost [10,11]. Hence, considerable effort is being devoted to developing inexpensive electrode materials with high specific capacitance. Among various materials investigated, nickel- and cobalt-based materials, including NiO, CoO_x, $Ni(OH)_x$, and $Co(OH)_x$, are of interest as inexpensive replacements for ruthenium oxide-based supercapacitors. It has been reported that nickel–cobalt binary metal oxides such as nickel cobaltite ($NiCo_2O_4$), have greater electronic conductivity and electrochemical activity than nickel and cobalt oxides [12]. $NiCo_2O_4$ is expected to offer richer redox chemistry than the two single component oxides due to the combined contributions from both nickel and cobalt ions; it is attractive for electrocatalytic water splitting [13] and lithium ion batteries [14]. However, it has received much less attention for supercapacitor applications [15,16].

In many applications, particle properties, such as size, surface area and crystallinity, have a profound effect on the performance of the materials. Methods that have been employed for the manufacture of nickel cobaltite nanoparticles include hydroxide decomposition [17,18], nanocasting [19], electrodeposition [15], combustion [20], coprecipitation [21] and the sol–gel synthesis [22]. Many of these have drawbacks in that they are energy consuming, lengthy and involve multiple steps. Therefore, more environmentally friendly, faster, and energy-efficient synthetic methods for nanoparticle production are of interest. The traditional chemical method, namely chemical bath deposition (CBD),

* Corresponding author at: Department of Organic and Nano Engineering and Institute of Nano Science and Technology, Hanyang University, Seoul 133-791, Republic of Korea. Tel.: +82 2 2220 0499; fax: +82 2 2298 4101.
E-mail address: ahn@hanyang.ac.kr (H. Ahn).

0925-8388/$ – see front matter © 2011 Elsevier B.V. All rights reserved.
doi:10.1016/j.jallcom.2011.03.136

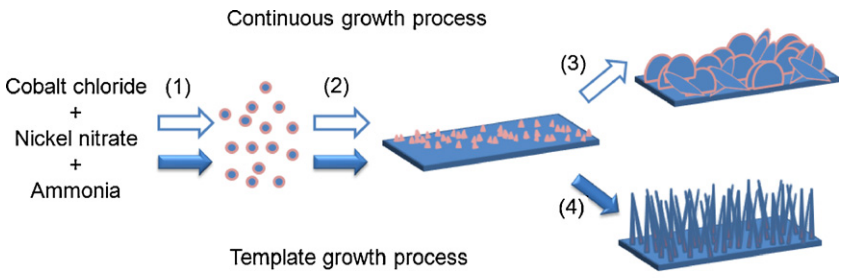

(1) Cobalt chloride/nickel nitrate mixture solution is heated to 70°C.

(2) Nuclei are produced on substrate surface.

(3) $NiCo_2O_4$ nanoflakes can be synthesized by the continuous growth process.

(4) Removing, drying and re-immersing in the solution at 70°C provides a template for growth of $NiCo_2O_4$ nanorods.

Fig. 1. Schematic depiction of growth processes for $NiCo_2O_4$ nanoflakes and nanorods.

has proven to be capable of controlling the size and morphology of materials by changing reaction parameters, such as temperature, pH and solvent concentration. Many unusual hierarchical structures of inorganic materials with high complexity and structural specialties can be created using the CBD method [23–28].

In the present work, we report a unique synthetic method in which $NiCo_2O_4$ porous morphologies (e.g., nanoflakes and nanorods) can be grown. The $NiCo_2O_4$ films have been characterized by a variety of techniques, including X-ray diffraction (XRD), X-ray photoelectron spectroscopy (XPS), Brunauer–Emmett–Teller (BET), field emission scanning electron microscopy (FESEM) and energy dispersive X-ray (EDX) analysis. The effect of the $NiCo_2O_4$ nanostructures on supercapacitor performance is examined by cyclic voltammetry and charge–discharge measurements, and specific capacitance values as high as 490 F g^{-1} are observed.

2. Experimental

Analytical grade chemicals $Ni(NO_3)_2{\cdot}6H_2O$ (99.999%), $CoCl_2{\cdot}6H_2O$ (99.999%) and KOH were purchased from Sigma–Aldrich and used without additional purification. An indium tin oxide (ITO) substrate was used as a current collector in the working electrode. Ammonia was slowly added to 0.1 M cobalt chloride and nickel nitrate solutions until the pH of the solutions reached 12. The two solutions were mixed to achieve 1:2 volumetric ratios of nickel and cobalt. During precipitation, heterogeneous reactions occurred at room temperature, and the deposition of mixed hydroxides took place on the substrate. The films were annealed at 300 °C in air for 3 h to convert the hydroxides into oxides. The weights of samples were measured by taking the difference of the weights of substrate before and after film deposition. The structure of the mixed metal oxides was examined by X-ray diffraction (Rigaku 2500) with CuKα radiation (λ = 1.5418 Å). The morphology of the $NiCo_2O_4$ was investigated by field emission scanning electron microscopy (Hitachi S4800). Compositional studies of the films have been carried out using EDX analysis. The BET specific surface areas were obtained from nitrogen adsorption/desorption isotherms recorded at −196 °C. A typical three-electrode experimental cell equipped with a working electrode, platinum counter electrode and Ag/AgCl reference electrode was used for measuring the electrochemical properties of the working electrode. All supercapacitor characterizations were carried out in 2 M aqueous KOH solution as an electrolyte. The cyclic voltammetry (CV) and charge–discharge (CD) studies were performed using a CHI 660D electrochemical workstation (CH instrument, USA). The XPS experiments were performed in an ESCALAB 220i-XL photoemission spectrometer with a monochromatic MgKα X-ray source ($h\nu$ = 1253.6 eV).

To control the morphology of $NiCo_2O_4$ nanostructures, two different synthetic processes were conducted. Fig. 1 shows a schematic illustration of the preparation of nickel–cobalt hydroxide nanoflake and nanorod hierarchical structures on ITO substrates prepared by the CBD method. For the synthesis of nickel–cobalt hydroxide nanoflakes, the cobalt chloride/nickel nitrate mixture solution was heated to 70 °C, and the substrate was kept in the solution until an adequate thickness (2 μm) of nanoflake structures had been deposited. For convenience, we refer to this as the "continuous growth process". In the case of the synthesis of nickel–cobalt hydroxide nanorod structures, a clean ITO substrate was immersed in the solution at room temperature and heated to 70 °C, but the ITO substrate was immersed only for 15 min and then removed from the solution and dried; this resulted in the formation of a thin nickel–cobalt hydroxide film on the ITO substrate. The thin nickel–cobalt hydroxide film was utilized as a template for growing the nickel–cobalt hydroxide nanorod structures. In the next step, the thin nickel–cobalt hydroxide film-covered ITO substrate was re-immersed in the solution at 70 °C and maintained until a thick nickel–cobalt hydroxide nanorod film was deposited. This second process is referred to as the "template growth process". After nickel–cobalt hydroxide film deposition, the substrate was removed from the solution and washed with doubly distilled water. Since the synthesized films are hydroxides, these films were annealed at 300 °C in air for 3 h to convert the hydroxides into oxides [18]. As evidenced by SEM, annealing did not cause a morphology change in the samples, so the growth mechanism of $NiCo_2O_4$ is the same with that for nickel–cobalt hydroxide.

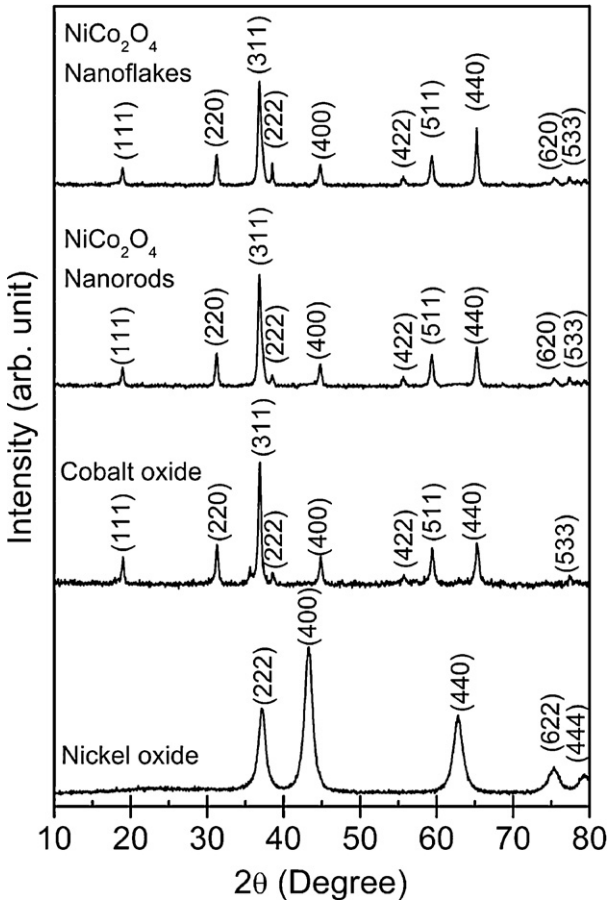

Fig. 2. X-ray diffraction patterns of NiO, Co_3O_4, $NiCo_2O_4$ nanoflake and nanorod samples annealed at 300 °C for 3 h.

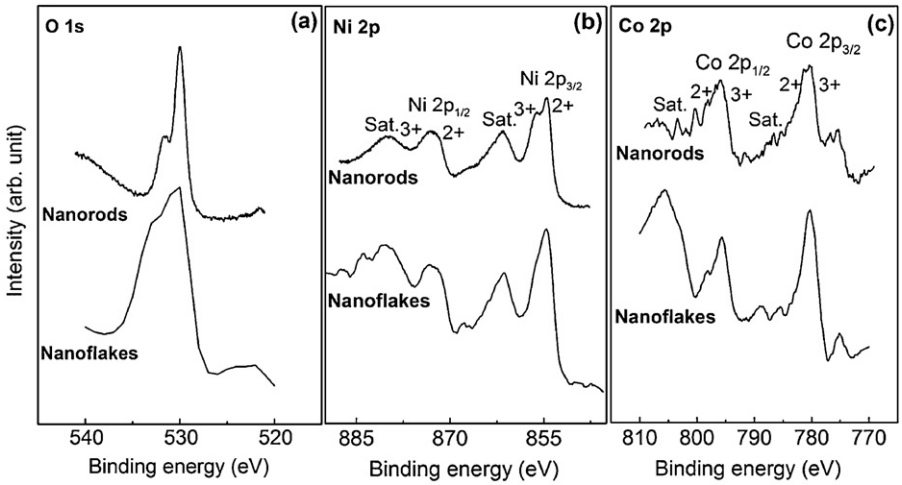

Fig. 3. XPS analysis of $NiCo_2O_4$ nanoflake and nanorod samples.

3. Results and discussion

3.1. X-ray diffraction analysis

In order to avoid intense ITO background peaks, powder X-ray diffraction analysis was performed to characterize the crystalline structures of the prepared nickel cobaltite films calcined at 300 °C for 3 h. Fig. 2 shows XRD patterns of nickel oxide, cobalt oxide, nickel cobaltite nanorod and nanoflake powder samples. As seen in the figure, all the samples have polycrystalline structures. The experimentally obtained XRD patterns for each sample exactly agree with PCPDF data (not shown here) for $NiCo_2O_4$ (no. 73-1702), Co_3O_4 (no. 78-1969) and NiO (no. 89-5881) without any collateral peaks, indicating high purity of the prepared samples. The XRD patterns are almost identical between nanoflakes and nanorods. However, the intensities of the peaks for the $NiCo_2O_4$ nanoflakes are larger than for the nanorods, indicating higher crystallinity of the nanoflakes. It is well known that specific capacitance decreases with increasing crystallanity. Therefore, the $NiCo_2O_4$ nanorods are expected to have larger specific capacitance than the $NiCo_2O_4$ nanoflakes. The broad XRD patterns of the $NiCo_2O_4$ film indicate that the size of $NiCo_2O_4$ crystal is in the nanometer range [15].

3.2. XPS analysis

The surface chemistry of each element on the surface was evaluated using X-ray photoelectron spectroscopy. As shown in Fig. 3, the XPS peak positions are very similar for the $NiCo_2O_4$ nanoflakes and nanorods. The XPS O1s peak can be resolved into two components (Fig. 3a). The component at 529.9 eV is typical of metal–oxygen bonds, while the component at 531.4 eV is associated with oxygen

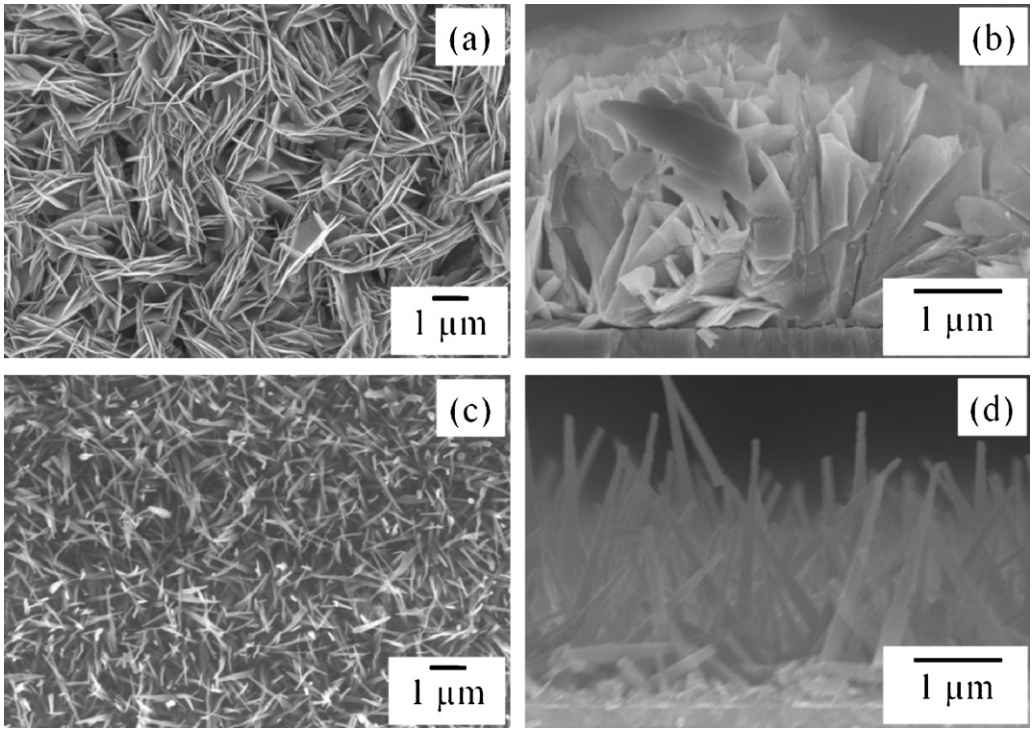

Fig. 4. FESEM top view images of (a) $NiCo_2O_4$ nanoflakes, (c) $NiCo_2O_4$ nanorods and cross-sectional views of (b) $NiCo_2O_4$ nanoflakes and (d) $NiCo_2O_4$ nanorods.

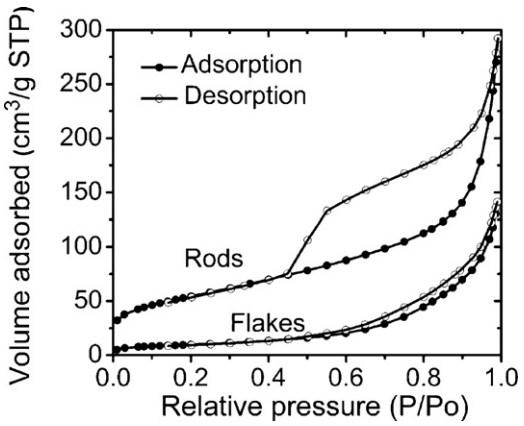

Fig. 5. Nitrogen adsorption/desorption isotherms of $NiCo_2O_4$ nanoflakes and nanorods.

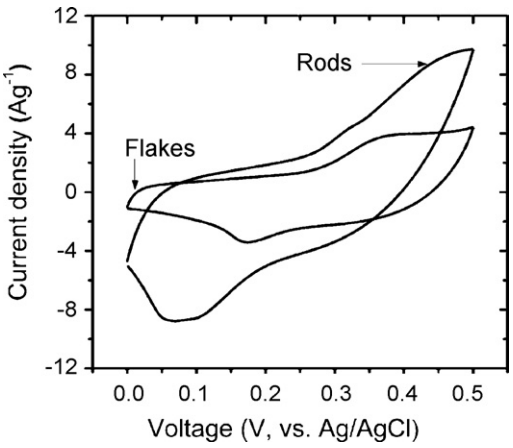

Fig. 6. Cyclic voltammograms of $NiCo_2O_4$ nanoflakes and nanorods at a scan rate of 20 mV s^{-1} in 2 M KOH solution.

ions in low coordination sites at the surface [18]. The XPS Ni 2p peak (Fig. 3b) consists of two spin-orbit doublets characteristic of Ni^{2+} and Ni^{3+} and two shake up satellites (identified as "Sat."). The XPS Co 2p peak (Fig. 3c) consists of two spin-orbit doublets characteristic of Co^{2+} and Co^{3+} and two shake up satellites [29]. Note that the shapes of the Co^{2+}/Co^{3+} and Ni^{2+}/Ni^{3+}peaks are slightly different for the nanoflakes and nanorods.

3.3. Surface morphological studies

Fig. 4a and c shows FESEM images of the $NiCo_2O_4$ films synthesized by the continuous growth process and template growth process, respectively. As seen in the figure, the $NiCo_2O_4$ nanoflakes and nanorods are obtained by the continuous growth process and template growth process, respectively. Cross-sectional views of the $NiCo_2O_4$ nanoflakes and nanorods are shown in Fig. 4b and d and indicate that both the $NiCo_2O_4$ nanoflakes and nanorods are grown almost vertically on the substrate, with lengths of about 2 μm. It is interesting to note that the shape of the nanorod is pointed at the end. Compared with the nanoflake-structured $NiCo_2O_4$ film (Fig. 4a), the nanorod-structured $NiCo_2O_4$ film exhibits much higher porosity. The relative proportions of nickel and cobalt in the nanoflake and nanorod films have been investigated using EDX analysis, and the Ni:Co atomic weight ratios in the $NiCo_2O_4$ nanorods and nanoflakes is 40:60 and 35:65, respectively.

3.4. BET surface area measurements

BET specific surface area measurements have been performed to measure the surface areas of the two $NiCo_2O_4$ nanostructures. Fig. 5 shows the nitrogen adsorption/desorption isotherms of the $NiCo_2O_4$ nanorods and nanoflakes. The adsorption curve gradually increases in the middle-pressure region and then increases abruptly in the high pressure region (>0.8 P/P_0; P/P_0: relative pressure). This behavior can be attributed to capillary condensation and multilayer adsorption of nitrogen in mesopores. The profile of the hysteresis loop for the $NiCo_2O_4$ nanorods indicates an adsorption/desorption characteristic of highly porous materials [30]. The BET surface area of the $NiCo_2O_4$ nanorods is 196 $m^2\,g^{-1}$, which is much larger than the value of 35 $m^2\,g^{-1}$ for $NiCo_2O_4$ nanoflakes. Note that the highly porous structure and high surface area of the electrode material are beneficial to supercapacitor performance because the ion transfer rate in a porous system, and the extent of electrode/electrolyte interfacial area, are determined by the porosity of the electrode material. Therefore, the $NiCo_2O_4$ nanorods are expected to exhibit significantly better electrochemical properties than the $NiCo_2O_4$ nanoflakes.

3.5. Supercapacitor studies

Electrochemical properties of the $NiCo_2O_4$ electrodes were investigated by cyclic voltammetry and galvanostatic charge–discharge experiments. Cyclic voltammograms were measured at a scan rate of 20 mV s^{-1} in 2 M KOH within a potential window ranging from 0 to +0.5 V (vs. Ag/AgCl). The electrochemical reaction of $NiCo_2O_4$ with the electrolyte can be written as follows:

$$NiCo_2O_4 + OH^- \leftrightarrow NiCo_2O_4||OH^- + NiCo_2O_4\text{–}OH \quad (1)$$

Here, $NiCo_2O_4||OH^-$ represents the electric double layer formed by the hydroxyl ion, and $NiCo_2O_4$–OH represents the product formed by the cathode reaction involving the hydroxyl ion [31]. Comparative CV studies of $NiCo_2O_4$ nanostructures (Fig. 6) indicate that the area of the CV curve for the $NiCo_2O_4$ nanorod film is larger than that of the$NiCo_2O_4$ nanoflake film, which is obviously due to the higher surface area of the former. The difference in the redox peak positions between nanoflakes and nanorods may be due to differences in the individual electronic transition of Co^{2+}, Co^{3+}, Ni^{2+}, and Ni^{3+} or the combined effect of transition states of $Co^{2+}/Co^{3+}$and Ni^{2+}/Ni^{3+}, which can be affected by morphology and crystallinity differences [15]. The specific capacitance (C) of the electrode can be calculated from the following equation,

$$\text{Specific capacitance(C)} = \frac{I}{(dV/dt)m} \quad (2)$$

where I is the current (A), dV/dt (mV s^{-1}) denotes the scan rate, and m is the mass of the electrode. The measured specific capacitance for $NiCo_2O_4$ nanorods is 490 F g^{-1}, while for $NiCo_2O_4$ nanoflakes it is 330 F g^{-1}. The present products (nanorods and nanoflakes) achieve high specific capacitance at a relatively high mass loading of at least 0.3 mg cm^{-2}. The high capacitance of the nanorods can be attributed not only to large mesopores in the nanorods, which favor fast ionic transport in pores, but also to large channels between the nanorods which reserve adequate electrolytes during the charge–discharge process. In addition, the lower crystallinity of the nanorod film may contribute to higher capacitance compared to the nanoflake film.

The supercapacitive performances of the $NiCo_2O_4$ samples were evaluated using charge–discharge curves in the voltage range of 0–0.4 V at 2 mA. While measuring charge–discharge data, an IR drop was observed in the voltage range 0–0.5 V. In order to avoid this, the charge–discharge study was performed in the 0–0.4 V range. Fig. 7a shows comparison of the charge–discharge curves of the $NiCo_2O_4$ nanorod and nanoflake films. The energy density (E) and

Table 1
Electrical parameters of $NiCo_2O_4$ supercapacitors obtained from the charge–discharge curves.

For $NiCo_2O_4$	I[a] (mA)	C_c[b] (s)	C_d[c] (s)	CDE[d] (%)	ED[e] (Wh kg^{-1})	PD[f] (kW kg^{-1})
Flakes	2	36	35	97	19	2
Rods	2	80	79	98	45	2

[a] I, current.
[b] C_c, charging time.
[c] C_d, discharging time.
[d] CDE, charge–discharge efficiency.
[e] ED, energy density.
[f] PD, power density.

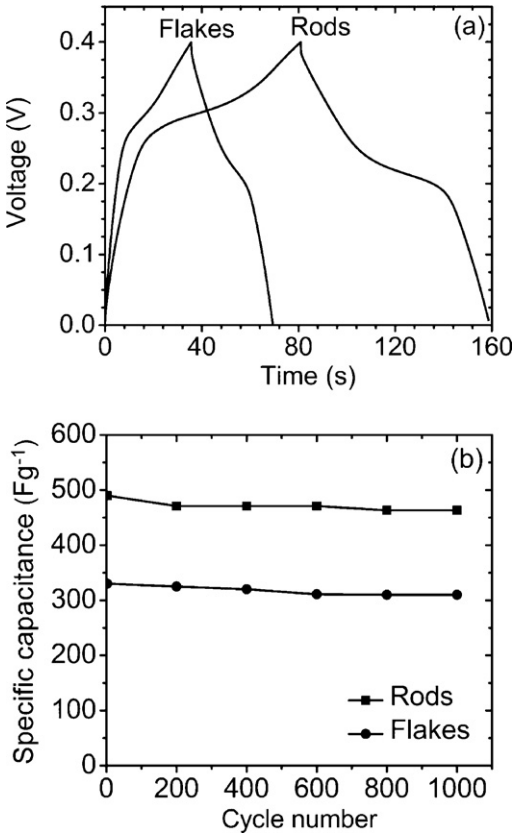

Fig. 7. (a) Charge–discharge curves of $NiCo_2O_4$ nanoflakes and nanorods; (b) stability test for $NiCo_2O_4$ nanoflakes and nanorods.

specific power (P) of the electrode is calculated using the following equations,

$$\text{Energy density}(E) = \frac{0.4\Delta t}{m} \quad (3)$$

$$\text{Power density}(P) = \frac{0.4I}{m} \quad (4)$$

where I is current in (A), m is weight of sample in (kg), 0.4 is the voltage range (V), Δt is the discharge time (s). The relationship between power density and energy density has been calculated from the charge–discharge curves. The electrical parameters obtained from the charge–discharge curves are summarized in Table 1. The charge and discharge times of the $NiCo_2O_4$ nanorods are much longer than those of the $NiCo_2O_4$ nanoflakes. The maximum energy density of 45 Wh kg^{-1} is obtained at a power density of 2 kW kg^{-1} for $NiCo_2O_4$ nanorods, which is higher than that of $NiCo_2O_4$ nanoflakes (19 Wh kg^{-1}). The stability and reversibility are also important for electrochemical superpcapacitor applications. Fig. 7 demonstrates the stability characteristics of deposited $NiCo_2O_4$ nanostructured samples as a function of the cycle number obtained from the cyclic voltammetry studies. A decrease of nearly 4% during the first 100 cycles (due to structural equilibration) and nearly 3% decrease after a subsequent 900 cycles are observed, which indicates reasonable stability characteristics for supercapacitor application.

The capacitance values obtained from the present study are lower than previously reported values [15,16]. The relatively low capacitances can be attributed to the anhydrous nature of the $NiCo_2O_4$ electrode, which depends on the preparation method, and the high electrical resistance of the ITO-coated glass substrate, which serves as the current collector.

4. Conclusions

In summary, a simple and cost-effective method has been demonstrated to synthesize hierarchical nanostructures of $NiCo_2O_4$. We have shown that the morphology of the $NiCo_2O_4$ nanostructures has a significant influence on supercapacitor performance and can easily be controlled by simply changing the synthetic process parameters. Although the chemical compositions of $NiCo_2O_4$ nanoflakes and nanorods are almost identical, $NiCo_2O_4$ nanorods exhibit higher capacitance and energy density than $NiCo_2O_4$ nanoflakes, due to their higher surface area, larger inner channel nanostructures and lower crystallinity. Therefore, it is envisioned that the newly proposed synthetic process can be developed into a versatile route to produce $NiCo_2O_4$ nanorod-based hierarchical structures for supercapacitor applications. Composites and more complex structures of $NiCo_2O_4$ may also find additional technological applications.

Acknowledgment

This work was financially supported by a grant (M2009010025) from the Fundamental R&D Program for Core Technology of Materials funded by the Ministry of Knowledge Economy (MKE), a grant (K20901000006-09E0100-00610) from the International Research & Development Program of the National Research Foundation of Korea (NRF) funded by the Ministry of Education, Science and Technology (MEST) of Republic of Korea and the research fund of Hanyang University (HYU-2011-T).

References

[1] C.C. Hu, K.H. Chang, M.C. Lin, Y.T. Wu, Nano Lett. (2006) 12.
[2] J.W. Long, B. Dunn, D.R. Rolison, H.S. White, Chem. Rev. 104 (2004) 4463.
[3] M.L. Anderson, R.M. Stroud, D.R. Rolison, Nano Lett. (2002) 235.
[4] C.R. Sides, C.R. Martin, Adv. Mater. 17 (2005) 125.
[5] K.H. Chang, C.C. Hu, Appl. Phys. Lett. 88 (2006) 193102.
[6] L. Dimesso, S. Jacke, C. Spanheimer, W. Jaegermann, J. Alloys Compd. 509 (2011) 3777.
[7] F. Tenga, S. Santhanagopalana, Y. Wangb, D.D. Meng., J. Alloys Compd. 499 (2010) 259.
[8] B.E. Convey, Electrochemical Supercapacitors, Scientific Fundamentals and Technological Applications, Kluwer Academic/Plenum Publishers, New York, 1997, p. 15.
[9] C.C. Hu, W.C. Chen, K.H. Chang, J. Electrochem. Soc. 151 (2004) A281.
[10] Z.S. Wu, D.W. Wang, W. Ren, J. Zhao, G. Zhou, F. Li, H.M. Cheng, Adv. Funct. Mater. 20 (2010) 3595.
[11] C.C. Hu, C.C. Wang, K.H. Chang, Electrochim. Acta 52 (2007) 2691.

[12] M.R. Tarasevich, B.N. Efremov, Electrodes of Conductive Metallic Oxides, Part A, Elsevier, USA, 1982, p. 227.
[13] B. Cui, H. Lin, J.B. Li, X. Li, J. Yang, J. Tao, Adv. Funct. Mater. 18 (2008) 1440.
[14] R. Alcntara, M. Jaraba, P. Lavela, J.L. Tirado, Chem. Mater. 14 (2002) 2847.
[15] V. Gupta, S. Gupta, N. Miura, J. Power Sources 195 (2010) 3757.
[16] T.Y. Wei, C.H. Chen, H.C. Chien, S.Y. Lu, C.C. Hu, Adv. Mater. 22 (2010) 347.
[17] B. Cui, H. Lin, Y. Liu, J. Li, P. Sun, X.C. Zhao, C.J. Liu, J. Phys. Chem. C113 (2009) 14083.
[18] J.F. Marco, J.R. Gancedo, M. Gracia, J.L. Gautier, E. RmHos, F.J. Berry, J. Solid State Chem. 153 (2000) 74.
[19] M. Cabo, E. Pellicer, E. Rossinyol, O. Castell, S. Surinach, M.D. Baro, Cryst. Growth Des. 9 (2009) 11.
[20] S. Verma, H.M. Joshi, T. Jagadale, A. Chawla, R. Chandra, S. Ogale, J. Phys. Chem. C112 (2008) 15106.
[21] D.G. Klissurski, E.L. Uzunova, Chem. Mater. 3 (1991) 1060.
[22] J.G. Kim, D.L. Pugmire, D. Battaglia, M.A. Langell, Appl. Surf. Sci. 162 (2000) 70.
[23] C.D. Lokhande, J.L. Gunjakar, A.M. More, J. Alloys Compd. 486 (2009) 570.
[24] R.R. Salunkhe, D.S. Dhawale, U.M. Patil, C.D. Lokhande, Sens. Actuators B 136 (2009) 39.
[25] U.M. Patil, S.B. Kulkerni, V.S. Jamdade, C.D. Lokhande, J. Alloys Compd. 509 (2011) 1677.
[26] D.P. Dubal, D.S. Dhawale, R.R. Salunkhe, S.M. Pawar, V.J. Fulari, C.D. Lokhande, J. Alloys Compd. 484 (2009) 218.
[27] D.P. Dubal, D.S. Dhawale, R.R. Salunkhe, V.S. Jamdade, C.D. Lokhande, J. Alloys Compd. 492 (2010) 26.
[28] D.K. Pawar, S.M. Pawar, P.S. Patil, S.S. Koleker, J. Alloys Compd. 509 (2011) 3587.
[29] A. Thissen, D. Ensling, M.F.J. Fernaĭndez, W. Jaegermann, R. Alcaĭntara, P. Lavela, J.L. Tirado, Chem. Mater. 17 (2005) 5202.
[30] L.B. Kong, M. Liu, J.W. Lang, Y.C. Luo, L. Kang, J. Electrochem. Soc. 156A (2009) 1000.
[31] D. Choi, G.E. Blomgren, P.N. Kumta, Adv. Mater. 18 (2006) 1178.